HHS Public Access

Author manuscript

Circ Res. Author manuscript; available in PMC 2024 February 10.

Published in final edited form as:

Circ Res. 2021 February 19; 128(4): e46–e62. doi:10.1161/CIRCRESAHA.120.317473.

Single-Cell Analysis of Blood-Brain Barrier Response to Pericyte Loss

Maarja A. Mäe[1,*], **Liqun He**[1,2], **Sofia Nordling**[1,3], **Elisa Vazquez-Liebanas**[1], **Khayrun Nahar**[1], **Bongnam Jung**[1,4], **Xidan Li**[5], **Bryan C. Tan**[6], **Juat Chin Foo**[7], **Amaury Cazenave-Gassiot**[7,8], **Markus R. Wenk**[7,8], **Yvette Zarb**[9], **Barbara Lavina**[1], **Susan E. Quaggin**[10], **Marie Jeansson**[1,5], **Chengua Gu**[11], **David L. Silver**[6], **Michael Vanlandewijck**[1,5], **Eugene C. Butcher**[3], **Annika Keller**[9], **Christer Betsholtz**[1,5,*]

[1]Immunology, Genetics and Pathology, Rudbeck Laboratory, Uppsala University, Dag Hammarskjölds väg 20, SE-751 85 Uppsala, Sweden

[2]Neurosurgery, Tianjin Medical University General Hospital, Tianjin Neurological Institute, Key Laboratory of Post-Neuroinjury Neuro-Repair and Regeneration in Central Nervous System, Ministry of Education and Tianjin City, Tianjin 300052, China

[3]Pathology, Stanford University School of Medicine, Stanford CA 94305, USA

[4]Present address: Harvard Medical School, Department of Surgery, Boston, MA 02115, USA

[5]Integrated Cardio Metabolic Center (ICMC) and Department of Medicine Huddinge, Karolinska Institutet Campus Flemingsberg, Blickagången 16, SE-141 57 Huddinge, Sweden

[6]Duke-NUS Medical School, 8 College Road, Singapore 169857

[7]Singapore Lipidomics Incubator (SLING), Life Sciences Institute, National University of Singapore

[8]Biochemistry, Yong Loo Lin School of Medicine, National University of Singapore

[9]Neurosurgery, Clinical Neuroscience Centrum, Zürich University Hospital, Zürich University, Frauenklinikstrasse 10, CH-8091

[10]Medicine, Northwestern University, Feinberg School of Medicine, Chicago, IL 60611, United States

[11]Neurobiology, Harvard Medical School, Boston.

Abstract

Address correspondence to: Dr. Christer Betsholtz, Professor of Vascular and Tumor Biology, Department of Immunology, Genetics and Pathology, Uppsala University, Dag Hammarskjölds väg 20, SE-751 85 Uppsala, Sweden, christer.betsholtz@igp.uu.se.
*To whom correspondence should be addressed.

AUTHOR CONTRIBUTIONS

M.A.M., A.K. and C.B. conceived and designed the project; M.A.M., E.V.L., K.N., M.V., B.J., B.C.T, J.C.F, A.C.G., M.R.W, Y.Z., B.L. performed experiments; L.H., S.N., K.B. and X.L. performed bioinformatic analysis; L.H. constructed the online database; S.E.Q., M.J., and C.G. provided essential reagents. M.A.M., C.B., L.H., S.N., E.B. analyzed the data; C.B. and M.A.M. wrote the manuscript with substantial input from L.H., S.N., E.B., D.S. and A.K. All authors reviewed and approved the manuscript.

COMPETING INTERESTS STATEMENT

The authors state no potential conflicts of interest with respect to the research, authorship, and/or publication of this article.

Rationale: Pericytes are capillary mural cells playing a role in stabilizing newly formed blood vessels during development and tissue repair. Loss of pericytes has been described in several brain disorders, and genetically induced pericyte deficiency in the brain leads to increased macromolecular leakage across the blood-brain barrier (BBB). However, the molecular details of the endothelial response to pericyte deficiency remain elusive.

Objective: To map the transcriptional changes in brain endothelial cells resulting from lack of pericyte contact at single-cell level, and to correlate them with regional heterogeneities in BBB function and vascular phenotype.

Methods and Results: We reveal transcriptional, morphological and functional consequences of pericyte absence for brain endothelial cells using a combination of methodologies, including single-cell RNA sequencing, tracer analyses and immunofluorescent detection of protein expression in pericyte-deficient adult *Pdgfb*$^{ret/ret}$ mice. We find that endothelial cells without pericyte contact retain a general BBB-specific gene expression profile, however, they acquire a venous-shifted molecular pattern and become transformed regarding the expression of numerous growth factors and regulatory proteins. Adult *Pdgfb*$^{ret/ret}$ brains display ongoing angiogenic sprouting without concomitant cell proliferation providing unique insights into the endothelial tip cell transcriptome. We also reveal heterogeneous modes of pericyte-deficient BBB impairment, where hotspot leakage sites display arteriolar-shifted identity and pinpoint putative BBB regulators. By testing the causal involvement of some of these using reverse genetics, we uncover a reinforcing role for angiopoietin 2 at the BBB.

Conclusions: By elucidating the complexity of endothelial response to pericyte deficiency at cellular resolution, our study provides insight into the importance of brain pericytes for endothelial arterio-venous zonation, angiogenic quiescence and a limited set of BBB functions. The BBB-reinforcing role of ANGPT2 is paradoxical given its wider role as TIE2 receptor antagonist and may suggest a unique and context-dependent function of ANGPT2 in the brain.

Graphical Abstract

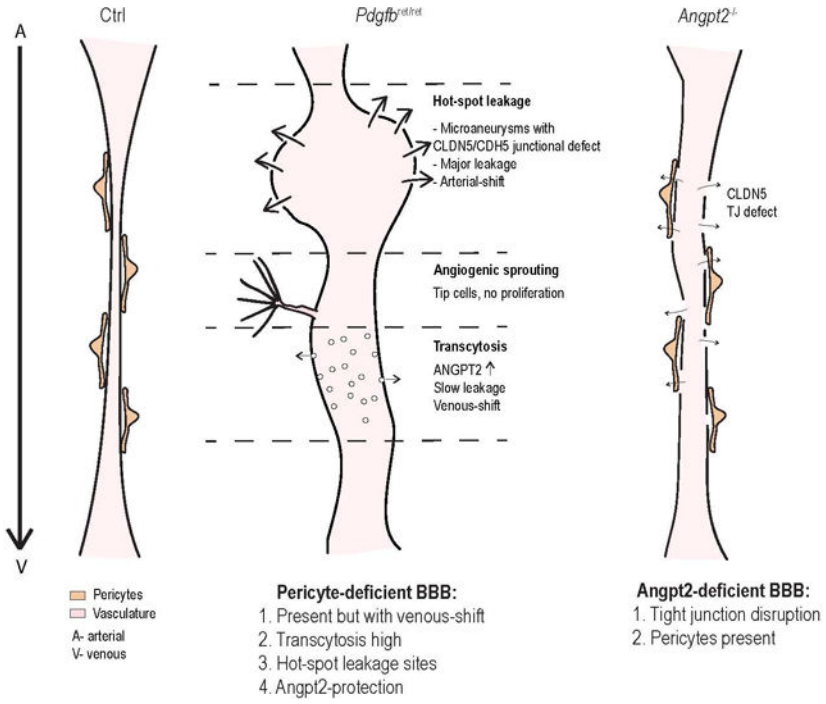

Keywords

pericyte; endothelial cells; blood-brain barrier; angiopoietin 2; permeability; endothelial junctions; endothelium; angiogenesis; single-cell RNA sequencing; neurovascular disease; Gene Expression and Regulation; Growth Factors/Cytokines; Pathophysiology; Vascular Biology

INTRODUCTION

Pericytes (PCs) and vascular smooth muscle cells (VSMCs), collectively referred to as vascular mural cells, form together with the endothelial cells (ECs) the cellular component of the blood vessel wall. While VSMCs surround arteries and veins and, depending on vessel type, regulate vascular tone and diameter, PCs are typically embedded within the basement membrane (BM) of blood capillaries, where they establish direct contacts with ECs.[1] PC morphology, distribution and density vary between organs and vascular beds. The central nervous system (CNS) microvasculature is considered to have a high PC density compared to peripheral organs,[2] suggesting a specific importance of PCs in the CNS. Indeed, studies suggest that PCs are critically required for the establishment of fully functional blood-brain and blood-retina barriers (BBB, BRB).[3–6] Developmental absence or reduction of PCs leads to increased endothelial transcytosis and misexpression of molecular transporters and leukocyte adhesion molecules.[3–6,7] A number of CNS diseases have been associated with PC loss or damage, including diabetic retinopathy,[8–10] stroke,[11] Alzheimer's disease,[12–14] amyotrophic lateral sclerosis[15] and aging.[16] However, whether PC damage contributes causally, and how and to what extent pericytes regulate the functional state of ECs in the pathogenesis of these conditions, are still not clear.

Platelet-derived growth factor-B (PDGFB) signaling through PDGF receptor-beta (PDGFRB) is essential for PC recruitment during developmental angiogenesis and postnatal survival in mice.[17,18] PC-deficient adult mice can however be generated through partial PDGFB/PDGFRB loss-of-function approaches. The most extensively PC-deficient brain microvasculature compatible with adult life observed so far occurs in mice carrying a homozygous deletion of the PDGFB heparan sulfate proteoglycan-binding motif (*Pdgfb*$^{ret/ret}$ mice).[19,20] These mice show increased BBB permeability, dysregulated CNS immune homeostasis, and defective para-vascular fluid transport, and they model the human genetic disease *primary familial brain calcification*.[3,7,21–26] Here, we characterize the EC consequences of PC loss in *Pdgfb*$^{ret/ret}$ mice using single-cell RNA-sequencing (scRNAseq) in combination with high-resolution imaging and genetic analyses of candidate molecular mediators of permeability changes. Our data show that PCs regulate EC identity and function in multiple ways. We identify two distinct modes of BBB breakdown in *Pdgfb*$^{ret/ret}$ mice and uncover an unexpected role of angiopoietin 2 (ANGPT2) at the BBB. Our data illustrate the power of scRNAseq to decode EC heterogeneity and provide a resource for the further analysis and interpretation of microvascular abnormalities in the adult brain.

METHODS

Data availability

The data that support the findings of this study are available from the corresponding author upon reasonable request. The single cell raw sequencing data and also processed counts table of our study are available from the NCBI Gene Expression Omnibus (GSE146007). Previously published wt EC scRNAseq dataset used in this study is also available in the GEO repository (GSE98816).

A complete description of the methods and reagents is provided in the Supplemental Material section.

RESULTS

A major proportion of the Pdgfb$^{ret/ret}$ cortical microvasculature is devoid of pericyte contact.

Constitutive *Pdgfb* knockout mice (*Pdgfb*$^{-/-}$) die perinatally displaying >95% loss of brain PCs.[17,27] By comparison, *Pdgfb*$^{ret/ret}$ mice[19] show 70–80% brain PC loss and survive postnatally (Figure 1A).[3] EC hyperplasia was reported in *Pdgfb*$^{-/-}$ embryos[28] but we concluded that overall EC numbers were normal in the adult *Pdgfb*$^{ret/ret}$ brain using immunofluorescent (IF) staining of EC nuclei by ERG (erythroblast transformation specific-related gene) antibodies (Online Figure IA). However, ECs formed a sparser network of vessels with increased diameter and numbers of ECs per vessel length in these mice (Figure 1A insets a,b and Online Figure IB).

We found numerous angiogenic sprouts with distinct tip cells[29] in adult *Pdgfb*$^{ret/ret}$ brains, whereas these were rarely seen in age-matched wildtype (WT, *Pdgfb*$^{+/+}$) or heterozygous (*Pdgfb*$^{ret/+}$) controls (Figure 1A inset c). By IF for ERG and PECAM1 (platelet endothelial cell adhesion molecule 1), we calculated the tip cell frequency to ≈0,6% of the total

EC number in *Pdgfb*$^{ret/ret}$ brain (Figure 1B). Labeling with EdU (ethynyl deoxyuridine) showed that the tip cells were not cycling (Online Figure IC,D), confirming previous observations in the developing mouse retina.[29] Neither overall cell proliferation, nor EC proliferation or death, the latter judged by cleaved caspase-3 IF, were significantly increased in *Pdgfb*$^{ret/ret}$ cerebral cortex (Online Figure ID,E). The unchanged turnover of ECs suggests that the observed angiogenic sprouting in *Pdgfb*$^{ret/ret}$ brains is either abortive (sprouts fail to establish patent capillary connections) or reflects a balanced formation and regression of vessel branches.

To assess PC morphology and density, we used IF analysis for aminopeptidase N (ANPEP) and two transgenic reporters: chondroitin sulfate proteoglycan 4 promoter-driven dsRED (*Cspg4*-dsRED) and PDGF receptor-beta promoter-driven green fluorescent protein (*Pdgfrb*-GFP)[30,31] in combination with Hoechst nuclear staining and EC detection by IF for ERG and PECAM1. These analyses showed that while residual PC in *Pdgfb*$^{ret/ret}$ were elongated, the PC:EC ratio in *Pdgfb*$^{ret/ret}$ cerebral cortex was ≈8-fold lower than in *Pdgfb*$^{ret/+}$ littermates (1:54 *vs.* 1:7) (Figure 1C-E) and >10-fold lower than separately bred *Pdgfb*$^{+/+}$ mice, where the PC:EC ratio was estimated to 1:4. The slight reduction in PC density in *Pdgfb*$^{ret/+}$ compared to *Pdgfb*$^{+/+}$ does not correlate with any obvious differences in vascular morphology and function, however, according to our previous analyses.[3]

Pdgfb$^{ret/ret}$ capillaries with residual PC contact showed a normalized diameter (Figure 1C), suggesting a direct effect of PCs on capillary diameter. While in *Pdgfb*$^{ret/ret}$ each PC contacted an extended capillary length, a major proportion (≈75%) of the capillary length remained devoid of visible PC contact. In contrast, both *Pdgfb*$^{ret/+}$ and WT mice showed PC contact along ≈100% of the brain capillary vessel length (Figure 1A), confirming previous observations.[32]

Although less severely than PCs, also VSMCs were affected in *Pdgfb*$^{ret/ret}$ brains. *Pdgfb*$^{ret/ret}$ arteries and veins maintain VSMCs coverage but we observed a reduction in the alpha-smooth muscle actin (αSMA a.k.a. ACTA2) staining of larger arteries (Online Figure IF), as well as a shift from circumferential to longitudinal orientation and reduced vessel coverage by VSMC at these sites.

Endothelial transformation and skewed arterio-venous zonation in Pdgfb$^{ret/ret}$ mice.

We applied scRNAseq analysis using fluorescence-activated cell sorting (FACS) and the SmartSeq2 protocol[33] to investigate how PC deficiency affects EC gene expression. We first generated *Pdgfb*$^{ret/+}$ and *Pdgfb*$^{ret/ret}$ mice carrying *Claudin 5* (*Cldn5*)-GFP and *Cspg4*-DsRed, transgenic reporters for EC and PC, respectively.[31,34] Messenger RNA contamination between ECs and PCs is frequently observed in public scRNAseq datasets,[35,36] likely reflecting that the two cell types, firmly adjoined by a common BM, are difficult to separate during tissue disintegration. We therefore used the double transgenic reporters to deselect contaminated cells during FACS.[37] Pure brain EC (*Cldn5*-GFP^{+}, *Cspg4*-DsRed^{-}) from 3-month-old mice were sorted into 384-well-plates and RNA-sequenced (Figure 2A).

1,187 quality-controlled single cell transcriptomes from *Pdgfb*$^{ret/+}$ and *Pdgfb*$^{ret/ret}$ mice were obtained and compared to scRNAseq data reported previously from WT mice of the same genetic background.[34,37] A total of 2,389 EC transcriptomes distributed into 9 clusters using the Pagoda2 package (Figure 2B).[38] Based on previously established markers for arterio-venous (A-V) zonation in the adult mouse brain,[34] some clusters were identified as arterial/arteriolar (#8 and 9), capillary (#4 and 6) or venous (#3) EC (Figure 2C). Gene Ontology (GO) analysis of cluster-enriched transcripts showed significantly different association with terms for biological processes such as vascular development (cluster #9), cell migration (cluster #8), molecular transport (cluster #6) and cell adhesion (cluster #3), implying functional differences related to A-V position (Online Figure IIA and Online Table I). Two clusters (#5 and #7) were characterized by high expression of immediate early genes (IEG) and interferon response genes (IRG), respectively, and the enriched transcriptomes of these two clusters were associated with GO terms encompassing metabolic processes (#5) and response to virus (#7), respectively (Online Figure IIA and Online Table I). We consider it likely that the IEG response was established during the experimental procedure as a result of cell stresses induced by tissue digestion. While we do not have an explanation for the underrepresentation of *Pdgfb*$^{ret/ret}$ cells in the IRG cluster, it is possible that it is caused by stochastic exposure to double-stranded RNA released from lysed cells.[34,39,40] Similar clusters have been observed in scRNAseq datasets from other organs[41], and they will not be discussed further herein. Finally, two clusters were enriched with transcripts that encode proteins associated with angiogenesis (#2) and growth factor signaling (#1). Because cluster #1 represents the strongest deviation from normal, we named this cluster “transformed”. The enriched transcriptomes of both clusters #1 and #2 were associated with GO terms for developmental processes and cell migration (Online Figure IIA and Online Table I), similar to the arterial cluster #9 in spite of differences in clustering and specific gene expression (see further below).

In a UMAP (uniform manifold approximation and projection) landscape, the arterial/arteriolar and venous clusters were located at opposite ends, separated by the capillary/venular clusters (Figure 2C). The transformed and angiogenic clusters (#1 and #2) were on the side of this trajectory, but closer to the capillary-venous clusters. The relative distribution of cells of the three genotypes (*Pdgfb*$^{ret/ret}$, *Pdgfb*$^{ret/+}$ and *Pdgfb*$^{+/+}$) in the different clusters showed that cluster #1 was almost completely composed of, and cluster #2 dominated by, *Pdgfb*$^{ret/ret}$ cells (Figure 2C,D and Online Figure IIB). Conversely, the microvascular clusters (capillaries #4, #6 and arterioles #8) were underrepresented with *Pdgfb*$^{ret/ret}$ cells (Figure 2D). The contribution of *Pdgfb*$^{ret/ret}$ cells to the arterial and venous clusters was instead roughly proportional to their overall representation in the dataset (≈25%), suggesting that the arterial and venous EC phenotypes remain comparably intact in the *Pdgfb*$^{ret/ret}$ brain (Figure 2D). Capillary EC distributed into two clusters (#4 and #6) with different proportions of *Pdgfb*$^{ret/+}$ and *Pdgfb*$^{+/+}$ cells, however, with similar marker expression and position in UMAP (Figure 2B,C). The cluster #4 *vs.* 6 assignment may therefore reflect a technical batch effect or minor quantitative gene expression differences provided by the two control genotypes. The most differentially expressed genes for each cluster are shown in Figure 2B. Lists of enriched genes for clusters #1–9 are provided in Online Table II.

The gene expression patterns of all genes across the clusters are available gene-by-gene as bar-plot data at https://betsholtzlab.org/Publications/RetECscRNAseq/database.html.

To define nearest-neighbor relationships between cells, we next applied trajectory space (tSpace) analysis, which recapitulates dynamic and spatial relationships better than UMAP in multiple organisms and processes.[42–44] tSpace defined three principal branches in our data, representing arterial, venous and angiogenic ECs, all joined by a centrally located population of capillary/microvascular cells (Figure 2E). The tSpace branches correspond roughly to the different corners of the UMAP landscape but provide clearer separation of mature *vs*. transformed/angiogenic subsets of EC.

Taken together, these analyses suggest that a major proportion (albeit not all) of the *Pdgfb*$^{ret/ret}$ brain microvascular ECs display a substantially transformed gene expression. In addition to the upregulated expression of molecules involved in angiogenesis and growth factor signaling, the cells of clusters #1 and #2 show decreased expression of certain transporters (*Mfsd2a, Tfrc, Slc16a1, Slc38a3*) (Figure 2B), suggesting that PC contact is required for ECs to assume and/or maintain certain specific BBB functions. Nevertheless, the phenotypic transformation of EC that we observe in the absence of PCs does not reflect a general loss of BBB markers. Many established BBB markers, including the tight junction molecule claudin 5 (*Cldn5*), the glucose transporter Glut 1 (*Slc2a1*), other influx transporters (*Slco1c1, Slco1a4, Slc40a1*), efflux transporters (*Abcb1a* a.k.a. P-glycoprotein) and the BBB-specific transcription factor *Zic3,* were all normally expressed (Online Figure III). Out of 64 CNS-specific EC markers[45] regulated by Wnt,[46] 20 were downregulated and 2 upregulated in *Pdgfb*$^{ret/ret}$ cells (Online Table III), but these changes were modest (2-fold or less). Moreover, up- and downregulation, respectively, of venous (*Slc38a5* and *Nrp2*) and capillary (*Mfsd2a, Slc16a1, Slc1a1*) markers[34] suggested venous skewing of the EC identity rather than loss of BBB functions (Online Figure IVA). To deepen the analysis of A-V zonation, we assessed 64 top venous and arterial markers of brain ECs[34] across the 9 clusters, confirming that *Pdgfb*$^{ret/ret}$ ECs are venous-shifted with several venous markers upregulated including *Nr2f2* and *Icam1* (Online Figure IVB). Although less conspicuously, some arterial markers were also upregulated, including *Bmx* and *Gkn3*, possibly suggesting a mixed A-V identity in the *Pdgfb*$^{ret/ret}$ microvasculature (Online Figure IVC).

To confirm the aberrant marker expression and disturbed A-V zonation in the *Pdgfb*$^{ret/ret}$ brain vasculature at the tissue level, we analyzed protein and transgenic reporter expression (Figure 2F,G and Online Figure IIC,D). Combined MFSD2A[34,47] and ANPEP[48,34] IF analysis showed that MFSD2A was lost specifically in EC devoid of PC contact (Figure 2F), suggesting that PCs control EC expression of MFSD2A directly through para- or juxtacrine signals. This conclusion was also supported by *Mfsd2a*-CreERT2-induced Ai9 reporter[49] expression, which labeled 84% of the capillary length in controls compared to 32% in *Pdgfb*$^{ret/ret}$ (Online Figure IIC,D). Similarly, expression of the capillary-venous markers solute carrier family 16 member 1 (SLC16A1) and transferrin receptor C (TFRC)[3,34] were focally lost in *Pdgfb*$^{ret/ret}$ brain microvessels (Figure 2G). Taken together, scRNAseq and tissue imaging show disturbed EC differentiation and A-V zonation in the *Pdgfb*$^{ret/ret}$ brain, implicating a critical role for PC in the establishment of proper vascular hierarchy in this organ.

Endothelial heterogeneity hallmarks the Pdgfb$^{ret/ret}$ microvasculature.

We next focused our attention to the cells of the transformed and angiogenic clusters (#1 and #2) dominated by *Pdgfb*$^{ret/ret}$ cells. A comparison between all *Pdgfb*$^{ret/ret}$ and all control (*Pdgfb*$^{ret/+}$ and *Pdgfb*$^{+/+}$) cells revealed almost 1,000 differentially expressed genes (Online Table IV; the top 25 up- or downregulated genes are shown in Online Figure V). Although a few cells in clusters #1 and #2 originated from *Pdgfb*$^{ret/+}$ and *Pdgfb*$^{+/+}$ controls, the *Pdgfb*$^{ret/ret}$ cells distinguished from these by being uniquely enriched with a number of transcripts, including fibroblast growth factor-binding protein-1 (*Fgfbp1*), connective tissue growth factor (*Ctgf*), bone morphogenetic protein (*Bmp*) *−4* and *−6* and *Angpt2* (Figure 3A). Intriguingly, high expression of these genes was seen also in the *Pdgfb*$^{ret/ret}$ cells present in the venous (#3) and capillary (#4) clusters (Figure 3A). *Fgfbp1* encodes a secreted protein that binds FGFs and promotes signaling through FGFRs,[50,51] and it has been functionally implicated in embryonic angiogenesis in the chick[52] and BBB development in the mouse.[53] *Fgfbp1* expression is high in mouse embryonic brain EC (our unpublished data) but negligible in adult brain EC.[34,36] Our results therefore suggest that the absence of PC causes a molecular transformation of capillary EC, including loss of markers for brain capillary specialization and concomitant gain of venous markers, as well as upregulation of transcripts normally expressed during development (*Fgfbp1*) or in pathological angiogenesis (*Angpt2*).

To explore the putative heterogeneity of the cells of clusters #1 and #2, we re-clustered them into 5 subclusters (*i-v* in Figure 3B). Subcluster *i*, comprising 90 cells, showed expression of several genes proposed as markers for tip cells, including *Mcam* and *Angpt2* (Figure 3C).[36,54–57] It also contained *Lamb1*-positive cells. IF analysis of MCAM and LAMB1 confirmed the specific expression of these two proteins in tip cells (Figure 3D). MCAM is expressed also by PCs[1], but at substantially lower level compared to tip cells (Figure 3D).

Not all cells in subcluster *i* were *Mcam* and *Lamb1* positive. To assess putative further heterogeneity in subcluster *i*, we sorted the transcriptomes uni-dimensionally using the SPIN algorithm (*s*orting *p*oints *i*nto *n*eighborhoods),[58] resulting in two groups, *i-1* and *i-2*, consisting of 7 and 83 cells, respectively (Figure 3E). *i-1* matched the expected tip cell profile, including expression of *Mcam* and *Lamb1* along with previously suggested tip cell markers *Cxcr4,*[56] *Pgf,*[59] *Kcna5, Sirpa*, and *Smoc2*.[45] GO analysis of *i-1* markers showed association with actin filament assembly and filopodia (Figure 3F) as expected for tip cells.[29] The number of *i-1* cells constituted 1.2% of the total number of analyzed *Pdgfb*$^{ret/ret}$ EC, i.e. roughly comparable to the tip cell frequency counted in *Pdgfb*$^{ret/ret}$ brain (0.6%).

Subcluster *ii* was enriched with capillary markers[34] (e.g. *Mfsd2a* and *Tfrc*) and dominated by *Pdgfb*$^{ret/ret}$ cells (Figure 3C). Subclusters *iii* and *iv* were enriched for venous markers[60] (e.g. *Nr2f2, Bmp4*) with *iv* displaying IEGs on top (Figure 3B), presumably reflecting gene activation during tissue dissociation, as discussed above. Subcluster *v* was positive for arteriolar EC markers[60] (*Gja4, Bmx, Gkn3, Sema3g*) (Figure 3B). Thus, the EC heterogeneity revealed through subcluster analysis appears to reflect in part a “shadow” A-V identity among the angiogenic and transformed ECs present in *Pdgfb*$^{ret/ret}$ brain. For complete lists of enriched genes for each subcluster, see Online Table V.

As a complement to the supervised assignment of A-V shadow identity using selected A-V marker distribution in subclusters, we also analyzed the relationships between subclusters *i-v* and their mature counterparts (global clusters #3–9) using unsupervised mutual nearest neighbor (MNN) alignment[61] and visualization in tSpace (Figure 3G-J and Online Figure VIA,B). MNN alignment provides batch correction, i.e. it subtracts global differences between genotypes, such as *Fgfbp1* and other genes hallmarking the *Pdgfb*$^{ret/ret}$ "batch" (Figure 3G,H). With this analysis, the transformed arterial cells stayed at more proximal locations in the arterial tSpace branch (weaker shadow identity) compared to the transformed venous cells, which distributed more distally into the venous branch (stronger shadow identity) (Online Figure VIA). The angiogenic EC were still positioned within their own branch after MNN alignment, with cluster *i-1* cells (tip cells) preferably at distal position (Figure 3I,J and Online Figure VIB). In conclusion, both supervised cluster annotation (Figure 3C) and unsupervised MNN alignment (Figure 3G-J and Online Figure VIA,B) suggested a heterogenous A-V shadow identity with venous preference among the transformed EC, and the presence of angiogenic EC with a distinguishable tip cell transcriptome.

Endothelial phenotypes correlate with BBB dysfunction.

The BBB leakage observed in *Pdgfb*$^{ret/ret}$ appears to be caused in part by endothelial transcytosis.[3] Systemically administered tracers between 1–200 kDa in size accumulate progressively in the *Pdgfb*$^{ret/ret}$ brain over 2–16 hours.[3] This accumulation is, however, uneven across the brain, which might reflect local differences in residual pericyte contact and/or different modes of BBB impairment in different vessel types along the A-V axis. We therefore set out to explore the correlation between gene expression and BBB dysfunction, focusing on subclusters *iii*, *iv* and *v,* which were dominated by ECs from *Pdgfb*$^{ret/ret}$ (Figure 3C). ANGPT2 is known to destabilize blood vessels through its antagonistic function at the tyrosine kinase receptor TIE2 (reviewed in[62]). MFSD2A on the other hand has a BBB-stabilizing role (its loss leads to increased brain endothelial transcytosis[63,64]), We therefore anticipated that subclusters *iii* and *iv*, in which *Angpt2* was high and *Mfsd2a* low, represented the ECs with the most extensively impaired BBB. However, by correlating the leakage of systemically administered 70 kDa tetramethylrhodamine (TMR)-dextran with ANGPT2 and MFSD2A expression in tissue sections, we instead found that the most extensive (hotspot) TMR-dextran leakage occurred at sites where both ANGPT2 and MFSD2A were low, i.e. corresponding to the gene expression pattern of subcluster *v* (Figure 3C). Thus, in addition to a broadly observable vesicular accumulation of TMR-dextran (Figure 4A) in ECs, consistent with transcytosis,[3] we detected hotspot leakage sites (Figure 4B). Neither type of leakage was observed in controls. Whereas areas with detectable transcytosis displayed MFSD2A expression (Figure 4A), only about 10% of the hotspot leakage sites had detectable MFSD2A (Figure 4B,C). ANGPT2 was barely detectable by IF staining in control brains, but strongly and heterogeneously expressed in *Pdgfb*$^{ret/ret}$ vessels, including but not limited to tip cells (Figure 4A,B). However, ANGPT2 was low or undetectable at most hotspot leakage sites (Figure 4B), and conversely, most sites with high ANGPT2 staining did not display hotspot leakage (Figure 4B). Quantifications revealed that only ≈11% of the hotspot leakage sites showed detectable ANGPT2 (Figure 4C). ANGPT2 expression was mainly observed in vessels devoid of mural cells, suggesting that it

depends on local rather than systemic cues (Figure 4D). Plasmalemma vesicle-associated protein (PLVAP) was upregulated at the mRNA level (*Plvap*) in *Pdgfb*$^{ret/ret}$ brains in subcluster *v* cells (Figure 3C) and an irregular PLVAP staining could be detected at a majority (59%, Figure 4C) of the hotspot leakage sites (Figure 4E). PLVAP is normally found in fenestrated blood vessels, including the capillaries of the brain's circum-ventricular organs, as exemplified by the organum vasculosum of the lamina terminalis and choroid plexus in the lateral ventricle, but otherwise not in the healthy BBB (Online Figure VIIA). Additionally, the leukocyte adhesion molecule, intercellular adhesion molecule 1 (*Icam1*) mRNA was upregulated in the *Pdgfb*$^{ret/ret}$ dominated subclusters *iii, iv,* and *v* (Figure 3C), a finding supported by ICAM1 protein detection by IF. In adult control brain, ICAM1 was detectably expressed mainly in veins and arteries (Figure 4F, and data not shown), whereas in *Pdgfb*$^{ret/ret}$, it was broadly upregulated in PC-deficient capillaries (Figure 4F and Online Figure VIIB,C). ICAM1 staining was observed at most (92%, Figure 4C) of the hotspot leakage sites. We also found extravasated CD45-positive leukocytes in *Pdgfb*$^{ret/ret}$ brains (but not in controls) often clustered at hotspot leakage sites (Online Figure VIID). Finally, we observed abnormal and irregular patterns of the adherens and tight junction proteins VE-cadherin (CDH5) and CLDN5 at hotspot leakage sites devoid of mural cells (Figure 4G,H), suggesting that EC junctions are altered at these sites.

Collectively, these results suggest two distinct modes of BBB dysfunction in *Pdgfb*$^{ret/ret}$. On the one hand hotspot leakage sites devoid of PC clearly visible by 70 kDa TMR-dextran extravasation; these sites were characterized by an arteriolar EC expression profile (subcluster *v* in Figure 3C), disturbed junctions, low or missing expression of MFSD2A, upregulated ICAM1 expression, extravasation of leukocytes, and ectopic PLVAP expression. On the other hand, the previously characterized increase in vesicular transcytosis across the EC in *Pdgfb*$^{ret/ret}$ brain;[3] this activated transport leads to widely distributed tracer leakage in *Pdgfb*$^{ret/ret}$ brains and seem to correlate with increased expression of a large number of mRNAs and proteins, including *Fgfbp1, Ctgf, Angpt2,* and *Bmp4.*

In order to provide mechanistic insight into the BBB leakage in *Pdgfb*$^{ret/ret}$ brain, we chose *Mfsd2a, Fgfbp1,* and *Angpt2* for further functional interrogation using reverse genetics. *Mfsd2a* was selected for study because it was downregulated in transformed EC in *Pdgfb*$^{ret/ret}$ and has been shown to suppress EC transcytosis in the intact BBB.[63,64] *Fgfbp1* was selected because it is the most strongly upregulated gene in *Pdgfb*$^{ret/ret}$ brain EC and has previously been implicated in BBB regulation.[52,53] *Angpt2*, finally, was selected because it is upregulated in *Pdgfb*$^{ret/ret}$ transformed EC and is known to enhance vascular permeability by antagonizing ANGPT1 signaling through TIE2.[62]

Loss of Mfsd2a or Fgfbp1 do not mediate major BBB permeability in Pdgfb$^{ret/ret}$ mice.

We compared the distribution of two tracers with different sizes, 1 kDa Alexa Fluor 555-(A555)-cadaverine (Figure 5A,B) and 70 kDa TMR-dextran (Figure 5C) following intravenous injection and circulation in adult awake *Mfsd2a*$^{-/-}$ or *Pdgfb*$^{ret/ret}$ mice. If MFSD2A mediates PC-suppressed EC transcytosis, we had expected to see similar or higher tracer leakage in *Mfsd2a*$^{-/-}$ than in *Pdgfb*$^{ret/ret}$ mice. However, under the experimental conditions used, neither tracer showed significantly increased accumulation

in *Mfsd2a*$^{-/-}$ compared to *Mfsd2a*$^{+/+}$ brains, in marked contrast to the strong leakage observed in *Pdgfb*$^{ret/ret}$ brains (Figure 5A-C). MFSD2A has been shown to be a critical lipid transporter at the BBB, responsible for the transport of the essential omega-3 fatty acid docosahexaenoic acid (DHA) into the brain,[47,65,66] and DHA levels in *Mfsd2a*$^{-/-}$ brains are markedly reduced compared to controls.[47] In spite of the reduced MFSD2A levels observed in *Pdgfb*$^{ret/ret}$ brain vessels, lipidomic analysis did not reveal detectable changes in lipid composition in *Pdgfb*$^{ret/ret}$ brains (Figure 5D), suggesting that the residual MFSD2A expression observed in these mice is sufficient to maintain DHA transport. Together, these observations demonstrate that the increased permeability of the *Pdgfb*$^{ret/ret}$ brain vasculature is caused by other mechanisms than loss of MFSD2A.

To address if the second candidate, FGFBP1, mediates or protects against the increased BBB permeability in *Pdgfb*$^{ret/ret}$ mice, we generated compound constitutive *Fgfbp1*$^{-/-}$;*Pdgfb*$^{ret/ret}$ mice and studied their vasculature in adult brains. Examining these mice for BBB permeability, we could not detect any increased leakage in single *Fgfbp1*$^{-/-}$ mice (*Pdgfb*$^{ret/+}$ background), nor could we detect increased leakage in double *Fgfbp1*$^{-/-}$:*Pdgfb*$^{ret/ret}$ *vs.* single *Pdgfb*$^{ret/ret}$ mutants (Online Figure VIII). From these data, we conclude that FGFBP1 does not cause BBB leakage in *Pdgfb*$^{ret/ret}$ mice, nor does it protect against it.

An unexpected role for Angpt2 at the BBB.

Although most of the strong sites of ANGPT2 expression observed in *Pdgfb*$^{ret/ret}$ mice did not co-localize with hotspot permeability sites (Figure 4B,C), *Angpt2*/ANGPT2 expression was generally increased in the EC of *Pdgfb*$^{ret/ret}$ brains (Figure 3A,4B,D and Online Figure VIID), particularly in EC devoid of PC contact (Figure 4D). To analyze if increased *Angpt2*/ANGPT2 expression contributes to the BBB defects observed in *Pdgfb*$^{ret/ret}$ mice, we induced deletion of *Angpt2* in *Pdgfb*$^{ret/ret}$ background. We generated *Pdgfb*$^{ret/ret}$:*Cdh5*-CreERT2:*Angpt2*$^{flox/flox}$ mice and induced deletion of *Angpt2* (*Pdgfb*$^{ret/ret}$;*Angpt2*^{iECKO}) by tamoxifen administration at 1 month of age, followed by analysis at 3 months of age. Contrary to our expectation, double *Pdgfb*$^{ret/ret}$;Angpt2^{iECKO} mutants were not protected against tracer leakage, but instead showed a marked increase in the brain accumulation of 1 kDa A555-cadaverine in comparison with single *Pdgfb*$^{ret/ret}$ mice (Figure 6A). IF staining confirmed the efficient depletion of ANGPT2 in *Pdgfb*$^{ret/ret}$;*Angpt2*^{iECKO} mutants (Figure 6B).

The aggravated tracer leakage in the *Pdgfb*$^{ret/ret}$;*Angpt2*^{iECKO} mice was unexpected in view of the reported role for ANGPT2 in vessel destabilization. To further address this paradoxical result, we analyzed constitutive *Angpt2* knockout mice (*Angpt2*$^{-/-}$ mice), which demonstrated that also single *Angpt2*$^{-/-}$ mice displayed abnormal brain vascular morphology and increased leakage of A555-cadaverine tracer (Figure 6D). The mural cell abundance and zonation judged by pericyte and VSMC marker expression was normal in *Angpt2*$^{-/-}$ mice, pointing to a different mechanism(s) of BBB disruption than in *Pdgfb*$^{ret/ret}$ mice (Figure 6E). We therefore focused our attention to EC junction morphology and the expression of markers of adherens junctions (CDH5) and tight junctions (CLDN5). While the distribution of both proteins confirmed the expected abnormalities in EC shapes, the *Angpt2*$^{-/-}$ vessels displayed specific alterations in the distribution of CLDN5, which

was both weaker and discontinuous along the cell-cell junctions, something that was not observed for CDH5 (Figure 6F). In contrast, control mice showed largely overlapping and continuous CDH5 and CLDN5 staining along the EC junctions. These data point to an important role for ANGPT2 in the development of CLDN5-containing tight junctions in the brain vasculature, as well as in maintenance of the integrity of these junctions during pericyte deficiency.

DISCUSSION

Our analysis provides detailed insight into how PC-deficiency changes the identity and behavior of brain EC in multiple ways with consequences for BBB integrity.

We found that the molecular A-V identity in EC was skewed in the PC-deficient brain. Out of 64 markers for brain venous EC, more than half were upregulated in *Pdgfb*$^{ret/ret}$ EC. Normally, a continuum of gene expression changes is observed along the A-V axis, including nested gene expression patterns of mRNAs coding for transcription factors, transporters and other protein classes.[34] This A-V zonation is likely a prerequisite for proper positioning of vascular functions along the A-V axis, such as molecular transport and immune cell trafficking. The mechanisms establishing endothelial zonation in the brain and elsewhere are generally not known, but our current findings suggest a role for PCs in this process.

We also addressed how PC-deficiency affects organotypic specialization in the brain EC, i.e. the molecular specification of the BBB phenotype. BBB function is impaired in the pericyte-deficient state,[3–5] but it has remained unclear how the PC-deficient BBB compares to other states of BBB-deficiency. Inhibition of Wnt signaling causes profound downregulation of BBB genes.[46] Our present results show that PC-deficiency have comparably modest effects on the BBB. Most major BBB markers were normally expressed in *Pdgfb*$^{ret/ret}$ mice, and where differences were observed, they seemed to reflect a venous-shifted rather than dismantled BBB. The lipid transporter MFSD2A is an interesting exception, as its expression in brain ECs requires direct PC contact. However, the reduced MFSD2A expression observed in *Pdgfb*$^{ret/ret}$ mice was sufficed to maintain a normal brain lipid composition, and it did also not explain the BBB leakage, which was far more extensive in *Pdgfb*$^{ret/ret}$ mice than in *Mfsd2a*$^{-/-}$ under our experimental conditions.

The finding of angiogenic sprouts and typical tip cells was surprising considering the general vascular rarefaction in the adult *Pdgfb*$^{ret/ret}$ brain. Analysis of EC cycling, apoptosis and total cell number suggested that the PC-deficient vessels were proliferatively quiescent. This provided us with an opportunity to molecularly characterize tip cells in absence of the concomitant vascular expansion that typically occurs during developmental and tumor angiogenesis. Indeed, we identified tip cells with a distinct gene and protein expression profile. While only a small number of tip cells was obtained, the depth of the SmartSeq2 technique provided meaningful information. To define markers unique for tip cells of the angiogenic sprout, we compared the tip (*i-1*) cells with the remaining cells (*i-2*) of the angiogenic cluster, which presumably include stalk cells. Of 112 enriched genes, 32 remained after multiple test correction. Clearly, this list is conservative. Moreover, because

tip and stalk cells are known to dynamically switch position during angiogenic sprouting,[67] some lag in transcriptional changes between tip cells and stalk cells would be expected, as also indicated by tSpace analysis, which positioned *i-1* cells preferably at the distal part of the angiogenic branch. Nevertheless, the 32-gene list of tip cell- *vs.* stalk cell-enriched transcripts includes *Mcam* and *Lamb1*, as well as previously proposed markers (*Cxcr4,*[56] *Pgf,*[59] *Kcna5, Sirpa*, and *Smoc2*[45]) along with several novel and unannotated transcripts, including micro-RNAs without known function. The erythropoietin receptor (*Epor*) mRNA was among the most distinct tip cell markers in our dataset, which may be relevant in relation to the suggested roles for erythropoietin in tumor angiogenesis.[68] Intriguingly, many of the tip cell markers, including *Epor,* are shared with rare capillary-resident angiogenic precursors recently described in lymph nodes and other tissues.[42] The significance of this similarity remains to be investigated.

Previous analyses have established transcytosis as a major mode of tracer transport across the BBB in PC-deficient mice.[3,5] Our present analysis revealed extensive EC heterogeneity and a putative second mode of BBB impairment in *Pdgfb*$^{ret/ret}$ brains: hotspot leakage. By correlating mRNA profiles in the single-cell data with BBB permeability and protein expression patterns, we found that hotspot leakage sites had unique morphological and molecular characteristics, including the abnormal distribution of EC junctional molecules. Hotspot sites were hallmarked by low MFSD2A and low ANGPT2 expression. They also displayed high ICAM1 and detectable PLVAP, features of possible relevance for the observed focal extravasation of leukocytes.

The low ANGPT2 expression at the hotspot leakage sites in *Pdgfb*$^{ret/ret}$ brain was surprising as ANGPT2 is conceived mainly as a TIE2 receptor antagonist, promoting vascular destabilization and pro-inflammatory responses.[62, 69–75] However, ANGPT2 has also been shown to exert context-dependent TIE2 agonistic activity, particularly in lymphatic endothelium or lymphatic-like vessels.[76–78] While we had anticipated that the upregulated expression of ANGPT2 in *Pdgfb*$^{ret/ret}$ mice exacerbated the BBB impairment, our data implicated the opposite, because double *Pdgfb*$^{ret/ret}$;*Angpt2*^{iECKO} mice showed an aggravated rather than a rescued BBB function. That ANGPT2 exerts a protective rather than destabilizing function at the BBB was further supported by data from single *Angpt2*$^{-/-}$ mice, which showed increased tracer leakage, abnormal vascular morphology and weak irregular junctional staining for CLDN5. If this reflects an agonistic role of ANGPT2 at the TIE2 receptor specifically in a BBB microenvironment remains to be investigated. TIE2 agonistic functions of ANGPT2 have been demonstrated in lymphatic EC, where they were linked to low expression of the TIE2 phosphatase VEPTP (PTPRB).[77] However, our scRNAseq data showed normal *Ptprb* expression in *Pdgfb*$^{ret/ret}$ EC (https://betsholtzlab.org/Publications/RetECscRNAseq/database.html).

Another proposed mechanism for ANGPT2-TIE-2 agonistic function involves translocation of ANGPT2-TIE2-integrin complexes from the BM to cell junctions, resulting in their stabilization and agonistic signaling.[79] Whether a specific molecular composition of the brain vascular BM prevents binding to ANGPT2-TIE2-integrin complexes and instead promotes a junctional location with resulting stabilization and reinforcement of CLDN5-containing tight junctions remains an intriguing possibility for further study.

It is increasingly appreciated that primary vascular dysfunction may cause or accelerate neurological disease.[80, 81] Conversely, neurodegenerative diseases may negatively affect brain vascular function.[82–84] Among the emerging links between neurodegenerative and cerebrovascular diseases, PC have received special attention.[85] PC loss or dysfunction correlate with a wide range of neurological and neurodegenerative conditions, including diabetic retinopathy,[8] Alzheimer's and other neurodegenerative diseases,[12–15, 86–89] aging[16] and stroke.[90] Mouse models of PC deficiency involving loss-of-function mutations in the *Pdgfb* or *Pdgfrb* genes or PC ablation by diphtheria toxin[91] display impaired BBB function,[3–5] reduced oxygen supply to the brain[91, 92] and myelin degradation.[93] Hypomorphic *Pdgfb* mice also mimic *primary familial brain calcification* in humans[23, 24] and display neurotoxic astrocyte activity and altered behavior and cognition suggestive of neuronal damage.[25] While all these studies point to a role for PC in overall brain function, it has remained unclear how PC deficiency affects their nearest neighbors, the ECs, at a molecular level. We undertook the present study using the most extensive, yet adult viable, mouse model of primary PC deficiency known, namely $Pdgfb^{ret/ret}$ mice,[3, 19, 20] in which ≈85% of the brain PC are lost, causing ≈75% of the capillary length to be devoid of visible PC contact. Because a the $Pdgfb^{ret/ret}$ brain vasculature is sufficiently functional to support general brain functions and adult life, these mice are particularly suitable for analysis of how the EC phenotype changes when PC contact is missing. Our data show that the EC response to PC loss is complex, as may be expected also in aforementioned diseases. Our herein reported data and the appended online database https://betsholtzlab.org/Publications/RetECscRNAseq/database.html should guide further studies of pathogenic vascular states and their consequences in brain disease.

Supplementary Material

Refer to Web version on PubMed Central for supplementary material.

ACKNOWLEDGEMENTS

This study was supported by the Swedish Research Council (C.B.: 2015-00550), the European Research Council (C.B.: AdG294556), the National Natural Science Foundation of China (L.H.: 81870978), the Leducq Foundation (C.B.: 14CVD02), the Swedish Cancer Society (C.B.:150735), Knut and Alice Wallenberg Foundation (C.B.: 2015.0030), Innovative Medicines Initiative (C.B.: IM2PACT-807015), the Swedish Society for Medical Research and Stanford Dean's Fellowship (S.N.) and NIH grants (E.C.B.: R01 AI130471 and CA228019). National Research Foundation grants, Singapore NRF2016NRF-NRFI001-15 and OF-IRG MOH-000217 (D.L.S.). The computations were performed on resources provided by Swedish National Infrastructure for Computing through Uppsala Multidisciplinary Center for Advanced Computational Science (UPPMAX) under Project SNIC 2017/7–240 and sllstore2017069. We thank C. Olsson, H. Leksell, P. Peterson and J. Chmielniakova for technical help.

Nonstandard Abbreviations and Acronyms:

ACTA2	alpha-smooth muscle actin
ANGPT2	angiopoietin 2
ANPEP	aminopeptidase N
A-V	arterio-venous
BBB	blood-brain barrier

BM	basement membrane
BMP	bone morphogenetic protein
BRB	blood-retina barrier
CDH5	vascular endothelial cadherin
CLDN5	claudin 5
CNS	central nervous system
CSPG4	chondroitin sulfate proteoglycan 4
CTGF	connective tissue growth factor
DHA	docosahexaenoic acid
EC(s)	endothelial cell(s)
EdU	ethynyl deoxyuridine
ERG	erythroblast transformation specific-related gene
FACS	fluorescence-activated cell sorting
FGFBP1	fibroblast growth factor-binding protein 1
GFP	green fluorescent protein
GO	gene ontology
ICAM1	intercellular adhesion molecule 1
IEG	immediate early genes
IF	immunofluorescence
IRG	interferon response genes
MFSD2A	major facilitator superfamily domain containing 2
MNN	mutual nearest neighbor
PC(s)	pericyte(s)
PDGF-B	platelet-derived growth factor B
PDGFRb	platelet-derived growth factor receptor beta
PC:EC	pericyte:endothelial cell ratio
PECAM1	platelet endothelial cell adhesion molecule 1
PLVAP	plasmalemma vesicle-associated protein
scRNAseq	single cell RNA sequencing

SLC16A1	solute carrier family 16 member 1
SPIN	sorting points into neighborhoods
TEK	tyrosine kinase receptor TIE2
TMR	tetramethylrhodamine
TFRC	transferrin receptor C
tSpace	trajectory space
UMAP	uniform manifold approximation and projection
VSMCs	vascular smooth muscle cells
WT	wild type

REFERENCES

1. Armulik A, Genove G and Betsholtz C. Pericytes: developmental, physiological, and pathological perspectives, problems, and promises. Dev Cell. 2011;21:193–215. doi:10.1016/j.devcel.2011.07.001. [PubMed: 21839917]
2. Sims DE. The pericyte--a review. Tissue Cell. 1986;18:153–74. doi:10.1016/0040-8166(86)90026-1. [PubMed: 3085281]
3. Armulik A, Genove G, Mae M, et al. Pericytes regulate the blood-brain barrier. Nature. 2010;468:557–61. doi:10.1038/nature09522. [PubMed: 20944627]
4. Bell RD, Winkler EA, Sagare AP, Singh I, LaRue B, Deane R and Zlokovic BV. Pericytes control key neurovascular functions and neuronal phenotype in the adult brain and during brain aging. Neuron. 2010;68:409–27. doi:10.1016/j.neuron.2010.09.043. [PubMed: 21040844]
5. Daneman R, Zhou L, Kebede AA and Barres BA. Pericytes are required for blood-brain barrier integrity during embryogenesis. Nature. 2010;468:562–6. doi:10.1038/nature09513. [PubMed: 20944625]
6. Park DY, Lee J, Kim J, et al. Plastic roles of pericytes in the blood-retinal barrier. Nat Commun. 2017;8:15296. doi:10.1038/ncomms15296. [PubMed: 28508859]
7. Török O, Schreiner B, Tsai H-C, et al. Pericytes regulate vascular immune homeostasis in the CNS. bioRxiv. 2019:644120. doi:10.1101/644120.
8. Bresnick GH, Davis MD, Myers FL and de Venecia G. Clinicopathologic correlations in diabetic retinopathy. II. Clinical and histologic appearances of retinal capillary microaneurysms. Arch Ophthalmol. 1977;95:1215–20. doi:10.1001/archopht.1977.04450070113010. [PubMed: 880082]
9. Enge M, Bjarnegard M, Gerhardt H, et al. Endothelium-specific platelet-derived growth factor-B ablation mimics diabetic retinopathy. EMBO J. 2002;21:4307–16. doi:10.1093/emboj/cdf418. [PubMed: 12169633]
10. Kusuhara S, Fukushima Y, Ogura S, Inoue N and Uemura A. Pathophysiology of Diabetic Retinopathy: The Old and the New. Diabetes Metab J. 2018;42:364–376. doi:10.4093/dmj.2018.0182. [PubMed: 30362302]
11. Fernandez-Klett F and Priller J. Diverse functions of pericytes in cerebral blood flow regulation and ischemia. J Cereb Blood Flow Metab. 2015;35:883–7. doi:10.1038/jcbfm.2015.60. [PubMed: 25853910]
12. Halliday MR, Rege SV, Ma Q, Zhao Z, Miller CA, Winkler EA and Zlokovic BV. Accelerated pericyte degeneration and blood-brain barrier breakdown in apolipoprotein E4 carriers with Alzheimer's disease. J Cereb Blood Flow Metab. 2016;36:216–27. doi:10.1038/jcbfm.2015.44. [PubMed: 25757756]
13. Miners JS, Schulz I and Love S. Differing associations between Abeta accumulation, hypoperfusion, blood-brain barrier dysfunction and loss of PDGFRB pericyte marker in the

precuneus and parietal white matter in Alzheimer's disease. J Cereb Blood Flow Metab. 2018;38:103–115. doi:10.1177/0271678X17690761. [PubMed: 28151041]

14. Sengillo JD, Winkler EA, Walker CT, Sullivan JS, Johnson M and Zlokovic BV. Deficiency in mural vascular cells coincides with blood-brain barrier disruption in Alzheimer's disease. Brain Pathol. 2013;23:303–10. doi:10.1111/bpa.12004. [PubMed: 23126372]
15. Winkler EA, Sengillo JD, Sullivan JS, Henkel JS, Appel SH and Zlokovic BV. Blood-spinal cord barrier breakdown and pericyte reductions in amyotrophic lateral sclerosis. Acta Neuropathol. 2013;125:111–20. doi:10.1007/s00401-012-1039-8. [PubMed: 22941226]
16. Montagne A, Barnes SR, Sweeney MD, et al. Blood-brain barrier breakdown in the aging human hippocampus. Neuron. 2015;85:296–302. doi:10.1016/j.neuron.2014.12.032. [PubMed: 25611508]
17. Lindahl P, Johansson BR, Leveen P and Betsholtz C. Pericyte loss and microaneurysm formation in PDGF-B-deficient mice. Science. 1997;277:242–5. doi:10.1126/science.277.5323.242. [PubMed: 9211853]
18. Hellstrom M, Kalen M, Lindahl P, Abramsson A and Betsholtz C. Role of PDGF-B and PDGFR-beta in recruitment of vascular smooth muscle cells and pericytes during embryonic blood vessel formation in the mouse. Development. 1999;126:3047–55. [PubMed: 10375497]
19. Lindblom P, Gerhardt H, Liebner S, et al. Endothelial PDGF-B retention is required for proper investment of pericytes in the microvessel wall. Genes Dev. 2003;17:1835–40. doi:10.1101/gad.266803. [PubMed: 12897053]
20. Abramsson A, Lindblom P and Betsholtz C. Endothelial and nonendothelial sources of PDGF-B regulate pericyte recruitment and influence vascular pattern formation in tumors. J Clin Invest. 2003;112:1142–51. doi:10.1172/JCI18549. [PubMed: 14561699]
21. Munk AS, Wang W, Bechet NB, et al. PDGF-B Is Required for Development of the Glymphatic System. Cell Rep. 2019;26:2955–2969 e3. doi:10.1016/j.celrep.2019.02.050. [PubMed: 30865886]
22. Zarb Y, Nassiri S, Utz SG, et al. Microglia control small vessel calcification via TREM2. bioRxiv. 2019:829341. doi:10.1101/829341.
23. Vanlandewijck M, Lebouvier T, Andaloussi Mae M, et al. Functional Characterization of Germline Mutations in PDGFB and PDGFRB in Primary Familial Brain Calcification. PLoS One. 2015;10:e0143407. doi:10.1371/journal.pone.0143407.
24. Keller A, Westenberger A, Sobrido MJ, et al. Mutations in the gene encoding PDGF-B cause brain calcifications in humans and mice. Nat Genet. 2013;45:1077–82. doi:10.1038/ng.2723. [PubMed: 23913003]
25. Zarb Y, Weber-Stadlbauer U, Kirschenbaum D, et al. Ossified blood vessels in primary familial brain calcification elicit a neurotoxic astrocyte response. Brain. 2019;142:885–902. doi:10.1093/brain/awz032. [PubMed: 30805583]
26. Nahar K, Lebouvier T, Andaloussi Mae M, Konzer A, Bergquist J, Zarb Y, Johansson B, Betsholtz C and Vanlandewijck M. Astrocyte-microglial association and matrix composition are common events in the natural history of primary familial brain calcification. Brain Pathol. 2020;30:446–464. doi:10.1111/bpa.12787. [PubMed: 31561281]
27. Leveen P, Pekny M, Gebre-Medhin S, Swolin B, Larsson E and Betsholtz C. Mice deficient for PDGF B show renal, cardiovascular, and hematological abnormalities. Genes Dev. 1994;8:1875–87. doi:10.1101/gad.8.16.1875. [PubMed: 7958863]
28. Hellstrom M, Gerhardt H, Kalen M, Li X, Eriksson U, Wolburg H and Betsholtz C. Lack of pericytes leads to endothelial hyperplasia and abnormal vascular morphogenesis. J Cell Biol. 2001;153:543–53. doi:10.1083/jcb.153.3.543. [PubMed: 11331305]
29. Gerhardt H, Golding M, Fruttiger M, et al. VEGF guides angiogenic sprouting utilizing endothelial tip cell filopodia. J Cell Biol. 2003;161:1163–77. doi:10.1083/jcb.200302047. [PubMed: 12810700]
30. He L, Vanlandewijck M, Raschperger E, et al. Analysis of the brain mural cell transcriptome. Sci Rep. 2016;6:35108. doi:10.1038/srep35108. [PubMed: 27725773]
31. Jung B, Arnold TD, Raschperger E, Gaengel K and Betsholtz C. Visualization of vascular mural cells in developing brain using genetically labeled transgenic reporter mice. J Cereb Blood Flow Metab. 2018;38:456–468. doi:10.1177/0271678X17697720. [PubMed: 28276839]

32. Grant RI, Hartmann DA, Underly RG, Berthiaume AA, Bhat NR and Shih AY. Organizational hierarchy and structural diversity of microvascular pericytes in adult mouse cortex. J Cereb Blood Flow Metab. 2019;39:411–425. doi:10.1177/0271678X17732229. [PubMed: 28933255]
33. Picelli S, Faridani OR, Bjorklund AK, Winberg G, Sagasser S and Sandberg R. Full-length RNA-seq from single cells using Smart-seq2. Nat Protoc. 2014;9:171–81. doi:10.1038/nprot.2014.006. [PubMed: 24385147]
34. Vanlandewijck M, He L, Mae MA, et al. A molecular atlas of cell types and zonation in the brain vasculature. Nature. 2018;554:475–480. doi:10.1038/nature25739. [PubMed: 29443965]
35. Schaum N, Karkanias J, Neff N, et al. Single-cell transcriptomics of 20 mouse organs creates a Tabula Muris. Nature. 2018;562:367–372. doi:10.1038/s41586-018-0590-4. [PubMed: 30283141]
36. Zeisel A, Hochgerner H, Lonnerberg P, et al. Molecular Architecture of the Mouse Nervous System. Cell. 2018;174:999–1014 e22. doi:10.1016/j.cell.2018.06.021. [PubMed: 30096314]
37. He L, Vanlandewijck M, Mae MA, et al. Single-cell RNA sequencing of mouse brain and lung vascular and vessel-associated cell types. Sci Data. 2018;5:180160. doi:10.1038/sdata.2018.160.
38. Fan J, Salathia N, Liu R, et al. Characterizing transcriptional heterogeneity through pathway and gene set overdispersion analysis. Nat Methods. 2016;13:241–4. doi:10.1038/nmeth.3734. [PubMed: 26780092]
39. van den Brink SC, Sage F, Vertesy A, Spanjaard B, Peterson-Maduro J, Baron CS, Robin C and van Oudenaarden A. Single-cell sequencing reveals dissociation-induced gene expression in tissue subpopulations. Nat Methods. 2017;14:935–936. doi:10.1038/nmeth.4437. [PubMed: 28960196]
40. Adam M, Potter AS and Potter SS. Psychrophilic proteases dramatically reduce single-cell RNA-seq artifacts: a molecular atlas of kidney development. Development. 2017;144:3625–3632. doi:10.1242/dev.151142. [PubMed: 28851704]
41. Kalucka J, de Rooij L, Goveia J, et al. Single-Cell Transcriptome Atlas of Murine Endothelial Cells. Cell. 2020;180:764–779 e20. doi:10.1016/j.cell.2020.01.015. [PubMed: 32059779]
42. Brulois K, Rajaraman A, Szade A, et al. A molecular map of murine lymph node blood vascular endothelium at single cell resolution. Nat Commun. 2020;11:3798. doi:10.1038/s41467-020-17291-5. [PubMed: 32732867]
43. Dermadi D, Bscheider M, Bjegovic K, Lazarus NH, Szade A, Hadeiba H and Butcher EC. Exploration of Cell Development Pathways through High-Dimensional Single Cell Analysis in Trajectory Space. iScience. 2020;23:100842. doi:10.1016/j.isci.2020.100842.
44. Xiang M, Grosso RA, Takeda A, et al. A Single-Cell Transcriptional Roadmap of the Mouse and Human Lymph Node Lymphatic Vasculature. Front Cardiovasc Med. 2020;7:52. doi:10.3389/fcvm.2020.00052. [PubMed: 32426372]
45. Sabbagh MF, Heng JS, Luo C, Castanon RG, Nery JR, Rattner A, Goff LA, Ecker JR and Nathans J. Transcriptional and epigenomic landscapes of CNS and non-CNS vascular endothelial cells. Elife. 2018;7. doi:10.7554/eLife.36187.
46. Phoenix TN, Patmore DM, Boop S, et al. Medulloblastoma Genotype Dictates Blood Brain Barrier Phenotype. Cancer Cell. 2016;29:508–522. doi:10.1016/j.ccell.2016.03.002. [PubMed: 27050100]
47. Nguyen LN, Ma D, Shui G, Wong P, Cazenave-Gassiot A, Zhang X, Wenk MR, Goh EL and Silver DL. Mfsd2a is a transporter for the essential omega-3 fatty acid docosahexaenoic acid. Nature. 2014;509:503–6. doi:10.1038/nature13241. [PubMed: 24828044]
48. Kunz J, Krause D, Kremer M and Dermietzel R. The 140-kDa protein of blood-brain barrier-associated pericytes is identical to aminopeptidase N. J Neurochem. 1994;62:2375–86. doi:10.1046/j.1471-4159.1994.62062375.x. [PubMed: 7910634]
49. Madisen L, Zwingman TA, Sunkin SM, et al. A robust and high-throughput Cre reporting and characterization system for the whole mouse brain. Nat Neurosci. 2010;13:133–40. doi:10.1038/nn.2467. [PubMed: 20023653]
50. Kurtz A, Wang HL, Darwiche N, Harris V and Wellstein A. Expression of a binding protein for FGF is associated with epithelial development and skin carcinogenesis. Oncogene. 1997;14:2671–81. doi:10.1038/sj.onc.1201117. [PubMed: 9178765]
51. Tassi E, Al-Attar A, Aigner A, Swift MR, McDonnell K, Karavanov A and Wellstein A. Enhancement of fibroblast growth factor (FGF) activity by an FGF-binding protein. J Biol Chem. 2001;276:40247–53. doi:10.1074/jbc.M104933200. [PubMed: 11509569]

52. Gibby KA, McDonnell K, Schmidt MO and Wellstein A. A distinct role for secreted fibroblast growth factor-binding proteins in development. Proc Natl Acad Sci U S A. 2009;106:8585–90. doi:10.1073/pnas.0810952106. [PubMed: 19433791]
53. Cottarelli A, Corada M, Beznoussenko GV, et al. Fgfbp1 promotes blood-brain barrier development by regulating collagen IV deposition and maintaining Wnt/beta-catenin signaling. Development. 2020;147. doi:10.1242/dev.185140.
54. del Toro R, Prahst C, Mathivet T, et al. Identification and functional analysis of endothelial tip cell-enriched genes. Blood. 2010;116:4025–33. doi:10.1182/blood-2010-02-270819. [PubMed: 20705756]
55. Heng JS, Rattner A, Stein-O'Brien GL, Winer BL, Jones BW, Vernon HJ, Goff LA and Nathans J. Hypoxia tolerance in the Norrin-deficient retina and the chronically hypoxic brain studied at single-cell resolution. Proc Natl Acad Sci U S A. 2019;116:9103–9114. doi:10.1073/pnas.1821122116. [PubMed: 30988181]
56. Strasser GA, Kaminker JS and Tessier-Lavigne M. Microarray analysis of retinal endothelial tip cells identifies CXCR4 as a mediator of tip cell morphology and branching. Blood. 2010;115:5102–10. doi:10.1182/blood-2009-07-230284. [PubMed: 20154215]
57. Zhao Q, Eichten A, Parveen A, et al. Single-Cell Transcriptome Analyses Reveal Endothelial Cell Heterogeneity in Tumors and Changes following Antiangiogenic Treatment. Cancer Res. 2018;78:2370–2382. doi:10.1158/0008-5472.CAN-17-2728. [PubMed: 29449267]
58. Tsafrir D, Tsafrir I, Ein-Dor L, Zuk O, Notterman DA and Domany E. Sorting points into neighborhoods (SPIN): data analysis and visualization by ordering distance matrices. Bioinformatics. 2005;21:2301–8. doi:10.1093/bioinformatics/bti329. [PubMed: 15722375]
59. Goveia J, Rohlenova K, Taverna F, et al. An Integrated Gene Expression Landscape Profiling Approach to Identify Lung Tumor Endothelial Cell Heterogeneity and Angiogenic Candidates. Cancer Cell. 2020;37:421. doi:10.1016/j.ccell.2020.03.002. [PubMed: 32183954]
60. Vanlandewijck M and Betsholtz C. Single-Cell mRNA Sequencing of the Mouse Brain Vasculature. Methods Mol Biol. 2018;1846:309–324. doi:10.1007/978-1-4939-8712-2_21. [PubMed: 30242769]
61. Haghverdi L, Lun ATL, Morgan MD and Marioni JC. Batch effects in single-cell RNA-sequencing data are corrected by matching mutual nearest neighbors. Nat Biotechnol. 2018;36:421–427. doi:10.1038/nbt.4091. [PubMed: 29608177]
62. Augustin HG, Koh GY, Thurston G and Alitalo K. Control of vascular morphogenesis and homeostasis through the angiopoietin-Tie system. Nat Rev Mol Cell Biol. 2009;10:165–77. doi:10.1038/nrm2639. [PubMed: 19234476]
63. Ben-Zvi A, Lacoste B, Kur E, Andreone BJ, Mayshar Y, Yan H and Gu C. Mfsd2a is critical for the formation and function of the blood-brain barrier. Nature. 2014;509:507–11. doi:10.1038/nature13324. [PubMed: 24828040]
64. Andreone BJ, Chow BW, Tata A, et al. Blood-Brain Barrier Permeability Is Regulated by Lipid Transport-Dependent Suppression of Caveolae-Mediated Transcytosis. Neuron. 2017;94:581–594 e5. doi:10.1016/j.neuron.2017.03.043. [PubMed: 28416077]
65. Alakbarzade V, Hameed A, Quek DQ, et al. A partially inactivating mutation in the sodium-dependent lysophosphatidylcholine transporter MFSD2A causes a non-lethal microcephaly syndrome. Nat Genet. 2015;47:814–7. doi:10.1038/ng.3313. [PubMed: 26005865]
66. Guemez-Gamboa A, Nguyen LN, Yang H, et al. Inactivating mutations in MFSD2A, required for omega-3 fatty acid transport in brain, cause a lethal microcephaly syndrome. Nat Genet. 2015;47:809–13. doi:10.1038/ng.3311. [PubMed: 26005868]
67. Jakobsson L, Franco CA, Bentley K, et al. Endothelial cells dynamically compete for the tip cell position during angiogenic sprouting. Nat Cell Biol. 2010;12:943–53. doi:10.1038/ncb2103. [PubMed: 20871601]
68. Annese T, Tamma R, Ruggieri S and Ribatti D. Erythropoietin in tumor angiogenesis. Exp Cell Res. 2019;374:266–273. doi:10.1016/j.yexcr.2018.12.013. [PubMed: 30576679]
69. Benest AV, Kruse K, Savant S, Thomas M, Laib AM, Loos EK, Fiedler U and Augustin HG. Angiopoietin-2 is critical for cytokine-induced vascular leakage. PLoS One. 2013;8:e70459. doi:10.1371/journal.pone.0070459. [PubMed: 23940579]

70. Fiedler U, Reiss Y, Scharpfenecker M, et al. Angiopoietin-2 sensitizes endothelial cells to TNF-alpha and has a crucial role in the induction of inflammation. Nat Med. 2006;12:235–9. doi:10.1038/nm1351. [PubMed: 16462802]
71. Fiedler U, Scharpfenecker M, Koidl S, Hegen A, Grunow V, Schmidt JM, Kriz W, Thurston G and Augustin HG. The Tie-2 ligand angiopoietin-2 is stored in and rapidly released upon stimulation from endothelial cell Weibel-Palade bodies. Blood. 2004;103:4150–6. doi:10.1182/blood-2003-10-3685. [PubMed: 14976056]
72. Hu J, Srivastava K, Wieland M, et al. Endothelial cell-derived angiopoietin-2 controls liver regeneration as a spatiotemporal rheostat. Science. 2014;343:416–9. doi:10.1126/science.1244880. [PubMed: 24458641]
73. Rathnakumar K, Savant S, Giri H, et al. Angiopoietin-2 mediates thrombin-induced monocyte adhesion and endothelial permeability. J Thromb Haemost. 2016;14:1655–67. doi:10.1111/jth.13376. [PubMed: 27241812]
74. Scharpfenecker M, Fiedler U, Reiss Y and Augustin HG. The Tie-2 ligand angiopoietin-2 destabilizes quiescent endothelium through an internal autocrine loop mechanism. J Cell Sci. 2005;118:771–80. doi:10.1242/jcs.01653. [PubMed: 15687104]
75. Ziegler T, Horstkotte J, Schwab C, et al. Angiopoietin 2 mediates microvascular and hemodynamic alterations in sepsis. J Clin Invest. 2013. doi:10.1172/JCI66549.
76. Kenig-Kozlovsky Y, Scott RP, Onay T, et al. Ascending Vasa Recta Are Angiopoietin/Tie2-Dependent Lymphatic-Like Vessels. J Am Soc Nephrol. 2018;29:1097–1107. doi:10.1681/ASN.2017090962. [PubMed: 29237738]
77. Souma T, Thomson BR, Heinen S, et al. Context-dependent functions of angiopoietin 2 are determined by the endothelial phosphatase VEPTP. Proc Natl Acad Sci U S A. 2018;115:1298–1303. doi:10.1073/pnas.1714446115. [PubMed: 29358379]
78. Thomson BR, Heinen S, Jeansson M, et al. A lymphatic defect causes ocular hypertension and glaucoma in mice. J Clin Invest. 2014;124:4320–4. doi:10.1172/JCI77162. [PubMed: 25202984]
79. Mirando AC, Shen J, Silva RLE, et al. A collagen IV-derived peptide disrupts alpha5beta1 integrin and potentiates Ang2/Tie2 signaling. JCI Insight. 2019;4. doi:10.1172/jci.insight.122043.
80. Iadecola C. The pathobiology of vascular dementia. Neuron. 2013;80:844–66. doi:10.1016/j.neuron.2013.10.008. [PubMed: 24267647]
81. Zhao Z, Nelson AR, Betsholtz C and Zlokovic BV. Establishment and Dysfunction of the Blood-Brain Barrier. Cell. 2015;163:1064–1078. doi:10.1016/j.cell.2015.10.067. [PubMed: 26590417]
82. Lendahl U, Nilsson P and Betsholtz C. Emerging links between cerebrovascular and neurodegenerative diseases-a special role for pericytes. EMBO Rep. 2019;20:e48070. doi:10.15252/embr.201948070. [PubMed: 31617312]
83. Sweeney MD, Sagare AP and Zlokovic BV. Blood-brain barrier breakdown in Alzheimer disease and other neurodegenerative disorders. Nat Rev Neurol. 2018;14:133–150. doi:10.1038/nrneurol.2017.188. [PubMed: 29377008]
84. Sweeney MD, Zhao Z, Montagne A, Nelson AR and Zlokovic BV. Blood-Brain Barrier: From Physiology to Disease and Back. Physiol Rev. 2019;99:21–78. doi:10.1152/physrev.00050.2017. [PubMed: 30280653]
85. Sweeney MD, Ayyadurai S and Zlokovic BV. Pericytes of the neurovascular unit: key functions and signaling pathways. Nat Neurosci. 2016;19:771–83. doi:10.1038/nn.4288. [PubMed: 27227366]
86. Baloyannis SJ and Baloyannis IS. The vascular factor in Alzheimer's disease: a study in Golgi technique and electron microscopy. J Neurol Sci. 2012;322:117–21. doi:10.1016/j.jns.2012.07.010. [PubMed: 22857991]
87. Farkas E and Luiten PG. Cerebral microvascular pathology in aging and Alzheimer's disease. Prog Neurobiol. 2001;64:575–611. doi:10.1016/s0301-0082(00)00068-x. [PubMed: 11311463]
88. Nation DA, Sweeney MD, Montagne A, et al. Blood-brain barrier breakdown is an early biomarker of human cognitive dysfunction. Nat Med. 2019;25:270–276. doi:10.1038/s41591-018-0297-y. [PubMed: 30643288]

89. Sagare AP, Sweeney MD, Makshanoff J and Zlokovic BV. Shedding of soluble platelet-derived growth factor receptor-beta from human brain pericytes. Neurosci Lett. 2015;607:97–101. doi:10.1016/j.neulet.2015.09.025. [PubMed: 26407747]

90. Fernandez-Klett F, Potas JR, Hilpert D, et al. Early loss of pericytes and perivascular stromal cell-induced scar formation after stroke. J Cereb Blood Flow Metab. 2013;33:428–39. doi:10.1038/jcbfm.2012.187. [PubMed: 23250106]

91. Nikolakopoulou AM, Montagne A, Kisler K, et al. Pericyte loss leads to circulatory failure and pleiotrophin depletion causing neuron loss. Nat Neurosci. 2019;22:1089–1098. doi:10.1038/s41593-019-0434-z. [PubMed: 31235908]

92. Kisler K, Nelson AR, Rege SV, et al. Pericyte degeneration leads to neurovascular uncoupling and limits oxygen supply to brain. Nat Neurosci. 2017;20:406–416. doi:10.1038/nn.4489. [PubMed: 28135240]

93. Montagne A, Nikolakopoulou AM, Zhao Z, et al. Pericyte degeneration causes white matter dysfunction in the mouse central nervous system. Nat Med. 2018;24:326–337. doi:10.1038/nm.4482. [PubMed: 29400711]

94. Kim D, Pertea G, Trapnell C, Pimentel H, Kelley R and Salzberg SL. TopHat2: accurate alignment of transcriptomes in the presence of insertions, deletions and gene fusions. Genome Biol. 2013;14:R36. doi:10.1186/gb-2013-14-4-r36. [PubMed: 23618408]

95. Liao Y, Smyth GK and Shi W. featureCounts: an efficient general purpose program for assigning sequence reads to genomic features. Bioinformatics. 2014;30:923–30. doi:10.1093/bioinformatics/btt656. [PubMed: 24227677]

96. Butler A, Hoffman P, Smibert P, Papalexi E and Satija R. Integrating single-cell transcriptomic data across different conditions, technologies, and species. Nat Biotechnol. 2018;36:411–420. doi:10.1038/nbt.4096. [PubMed: 29608179]

97. van Dijk D, Sharma R, Nainys J, et al. Recovering Gene Interactions from Single-Cell Data Using Data Diffusion. Cell. 2018;174:716–729 e27. doi:10.1016/j.cell.2018.05.061. [PubMed: 29961576]

98. Chan JP, Wong BH, Chin CF, et al. The lysolipid transporter Mfsd2a regulates lipogenesis in the developing brain. PLoS Biol. 2018;16:e2006443. doi:10.1371/journal.pbio.2006443.

NOVELTY AND SIGNIFICANCE

What Is Known?

- The blood-brain barrier (BBB) is a semipermeable layer of endothelial cells that selectively regulates solutes crossing into the extracellular fluid of the central nervous system where neurons reside.
- The BBB depends on signals from surrounding non-endothelial cell types, including the pericyte.
- Mice with low numbers of pericytes show increased passage of blood-borne molecules across the BBB.
- Several brain diseases have been associated with pericyte loss or damage and BBB disruption.

What New Information Does This Article Contribute?

- This study provides detailed information about how brain endothelial gene expression is reprogrammed when pericytes are missing.
- The expression of growth factors and pro-inflammatory mediators is increased, and the molecular profile is shifted from capillary to venous, while the BBB identity remains largely intact.
- Activated angiogenic sprouting without concomitant cell proliferation allowed identification of a specific molecular profile of endothelial tip cells.
- A new mode of BBB impairment induced by pericyte deficiency was uncovered, i.e. focal hotspot leakage sites with distinct gene and protein expression including the absence of angiopoietin 2 (Angpt2).
- *Angpt2* null mice show a specific defect in claudin 5-containing tight junctions, suggesting that Angpt2 signaling reinforces endothelial cell-cell contacts when they are challenged by pericyte loss.

Pericytes are obligatory cellular constituents of blood micro-vessels, but their function(s) remain poorly understood. Pericytes are particularly numerous in the brain and play a poorly defined role in the development and regulation of the BBB,. Numerous cerebral diseases have been associated with pericyte loss or damage, but whether this is causally pathogenic or a secondary effect is not clear. Using a mouse model with extensive brain pericyte hypoplasia, we studied how the absence of pericytes influences gene expression and function in brain endothelial cells. We found an extensive endothelial heterogeneity, including specific alterations in the expression of molecular transporters, a venous-shifted identity, the activation of angiogenic sprouting, and two distinct modes of BBB disruption, one widespread, involving vesicular transcytosis, and one focal, involving disrupted tight junctions. The latter (hotspot leakage sites) showed lowered expression of Angpt2, which first appeared paradoxical, since Angpt2 is primarily an endothelial destabilizing signal outside of the brain. However, *Angpt2* knockout mice demonstrated disrupted claudin 5-containing tight junctions in the brain, suggesting that

Angpt2 is necessary for proper BBB development, and that reduced Angpt2 expression triggers BBB disruption when pericytes are missing.

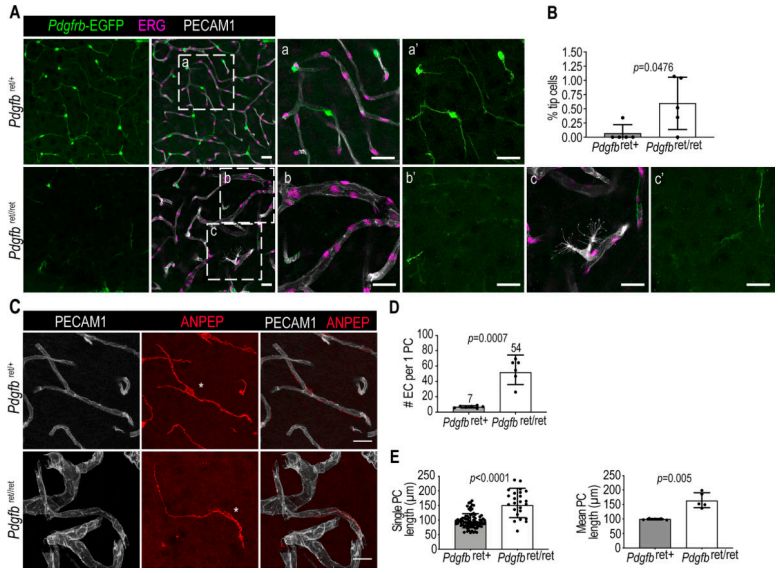

Figure 1. Vascular abnormalities in *Pdgfb*$^{ret/ret}$ mice.

A, IF and *Pdgfrb*-EGFP analysis of sagittal sections from adult brain cortex. Insets **a-c** illustrate vascular morphologies and cellular composition. Scale bars 25 µm. **B,** Quantification of tip cells per field as percentage of the total EC number (n=5, 6 fields per mouse). **C,** Representative confocal images of PC IF, asterisk marks the cell soma. Scale bar 20 µm.**D,** Quantification of PC:EC ratio (*Pdgfb*$^{ret/+}$ n=7 and *Pdgfb*$^{ret/ret}$ n=6, 6 fields per mouse). **E,** Quantification of PC length in cerebral cortex. Left graph illustrates the length range in all measured PC (n=5 mice, *Pdgfb*$^{ret/+}$ n=78 PC and *Pdgfb*$^{ret/ret}$ n=24 pericytes). Right graph shows mean PC length per mouse (n=5). In **D,E**, data was normally distributed and significance evaluated using unpaired two-tailed t-test with Welch's correction. In **B,D,F,G,J,** data was unevenly distributed and significance evaluated using non-parametric Mann Whitney test. In **B and D,** the data are presented as geometric mean ± geometric SD, and in **B,** as mean ± SD.

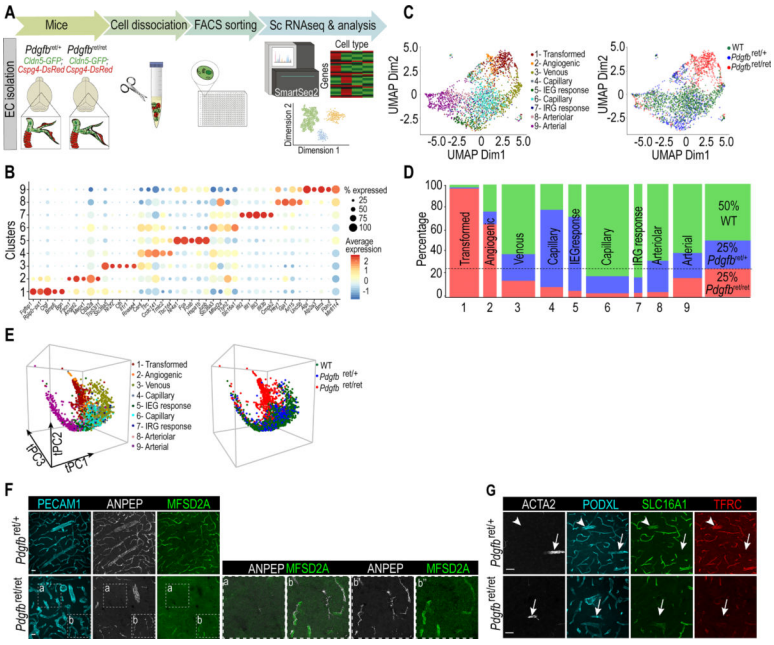

Figure 2. Transcriptomic changes in EC devoid of PC contact.

A, Schematic overview of EC isolation for scRNAseq. **B,** Dot plot of top markers for 9 Pagoda2 EC clusters. Dot size illustrates percentage of cells presenting transcript sequence count(s) and color illustrates the average expression level in the cells within a cluster. **C**, The 9 EC clusters from **B** visualized in a UMAP landscape (left), UMAP distribution by genotype (right). **D,** Genotype proportions in each cluster. Total proportion is shown in the right column. **E,** tSpace projections of all EC labeled by cluster assignment (left) and genotype (right). **F,G,** IF analysis of A-V marker expression as indicated. **F** inset **a** illustrates that EC devoid of PC lack MFSD2A expression. Inset **b** shows that EC with residual PC contact retain MFSD2A expression. Scale bar 25 μm. **G,** IF staining against the capillary/venous markers SLC16A1 and TFRC. PODXL (podocalyxin-like) stains all EC. Arrowheads point to veins and arrows to arterioles. Scale bar 40 μm.

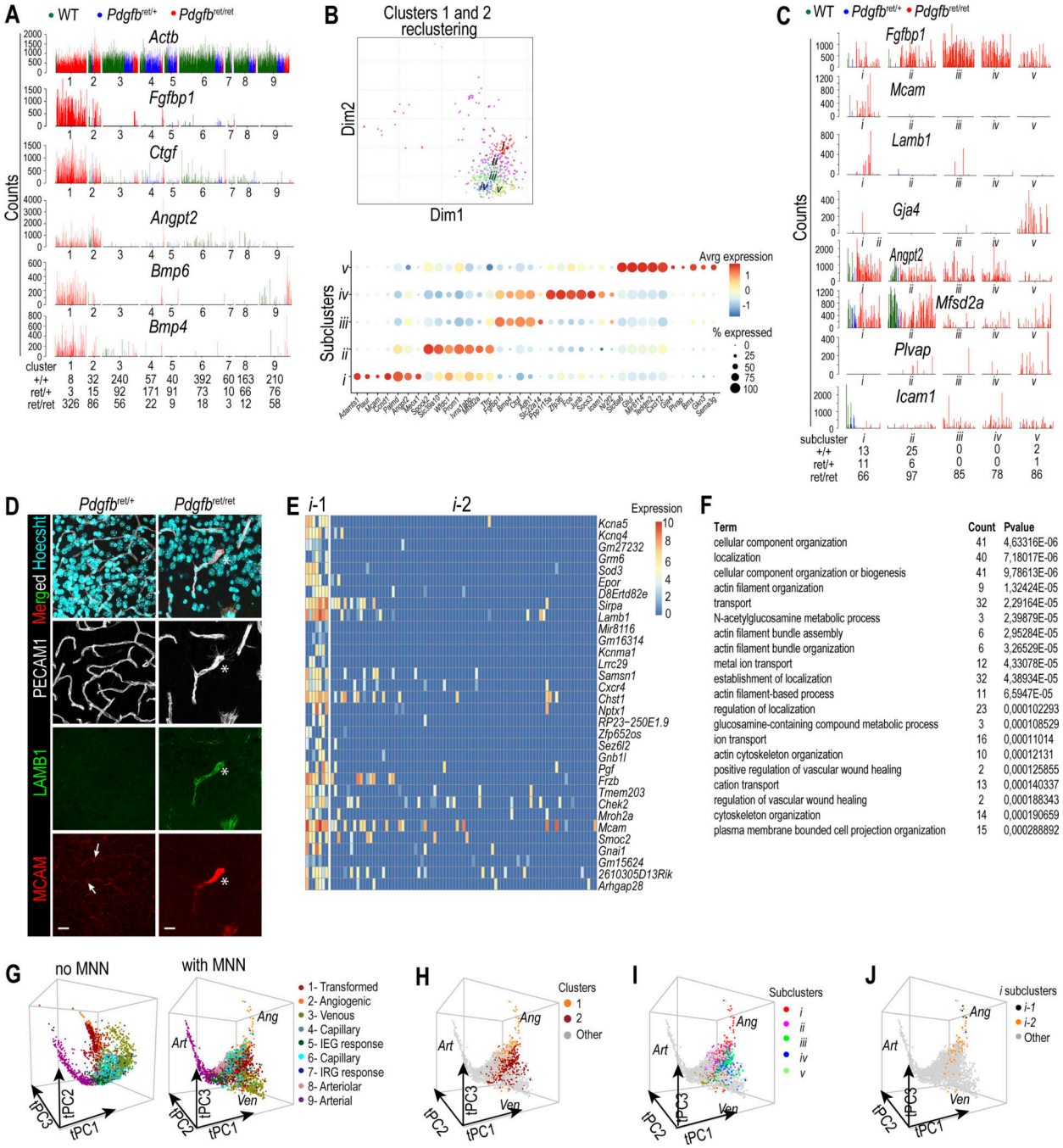

Figure 3. *Pdgfb*$^{ret/ret}$ EC heterogeneity.

A, ScRNAseq bar plots showing the expression of selected genes that are upregulated in clusters #1 and #2. **B, Upper panel:** Re-clustering of #1 and #2 results in 5 subclusters (*i-v).* **Lower panel:** Dot plot showing enriched genes for subclusters *i-v.* Dot size illustrates percentage of cells presenting transcript sequence count(s) and color illustrates the average expression level in the cells within a cluster. **C,** Bar plots of representative markers for each subcluster. **D,** IF visualization of tip cell (asterisk) in cerebral cortex. Arrows point at low-MCAM expressing PC. Scale bar 20 μm. **E,** Heatmap of *i-1*-enriched markers

across *i-1* and *i-2* cells sorted by SPIN. **F,** GO analysis of subcluster *i-1*-enriched genes. Terms for *biological process* are shown. **G-J,** tSpace projections. **G,** Supervised (left) and unsupervised (right) mutual nearest neighbor (MNN) alignment of EC by clusters. **H-J,** Cell distribution and gene expression in MNN-aligned graphs, as indicated. *Art*- arterial, *Ven*- venous, *Ang*- angiogenic.

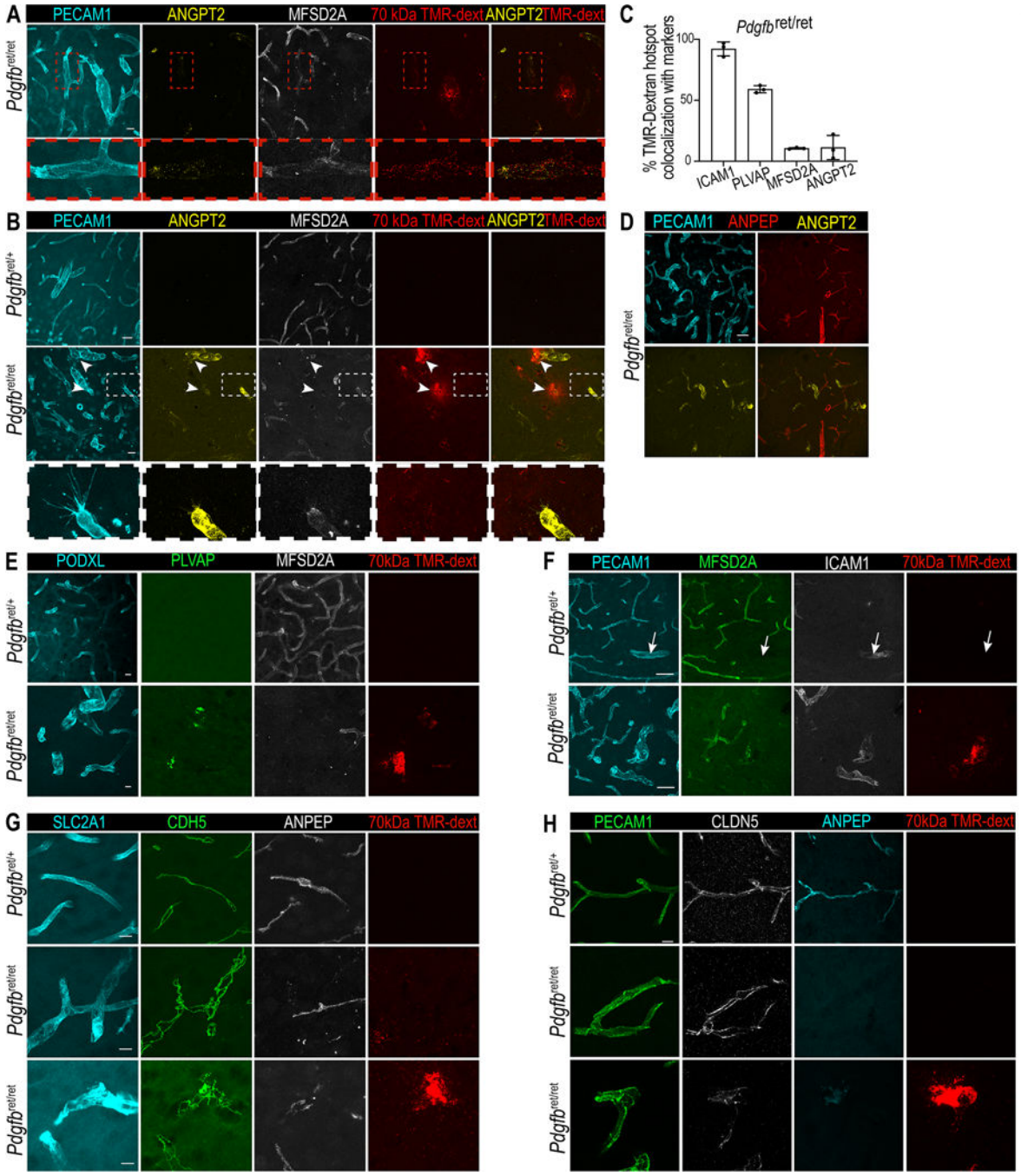

Figure 4. Hotspot leakage sites in *Pdgfb*$^{ret/ret}$ brains.

A,B, Confocal images of cerebral cortex of 70 kDa tetramethylrhodamine (TMR)-dextran (red) injected mice, together with IF staining for the indicated proteins **A,** Inset depicts MFSD2A^{low} vasculature with increased TMR-dextran positive vesicles (transcytosis). Scale bar 20 μm. **B,** Examples of TMR-dextran positive hotspot permeability sites (arrowheads). Inset shows ANGPT2-positive tip cell negative for TMR-dextran. Scale bar 20 μm. **C,** Quantification of colocalization between TMR-dextran hotspots and indicated markers (n=3). **D,** Upregulated ANGPT2 expression where PC contact is absent. Scale bar 40 μm. **E,**

Illustration of PLVAP staining at TMR-dextran positive hotspot permeability sites. Scale bar 20 μm. **F,** The majority of TMR-dextran positive hotspot permeability sites are MFSD2A-negative and ICAM1-positive. Scale bar 40 μm. **G,** Adherens junctions stained for CDH5 are thin and regular in controls (all EC stained by anti-glucose transporter type 1 (SLC2A1)), but discontinuous and irregular at TMR-dextran positive hotspot leakage sites. Adherens junctions at non-hotspot permeability sites are irregular but continuous (middle panel). ANPEP visualizes PC. Scale bar 10 μm. **H,** Tight junctions visualized using anti-CLDN5 staining are continuous in *Pdgfb*$^{ret/+}$ (all EC visualized by anti-PECAM1), but discontinuous and irregular at TMR-dextran positive hotspot leakage sites. Tight junctions in non-hotspot leakage sites in *Pdgfb*$^{ret/ret}$ are continuous (middle panel). Scale bar 10 μm.

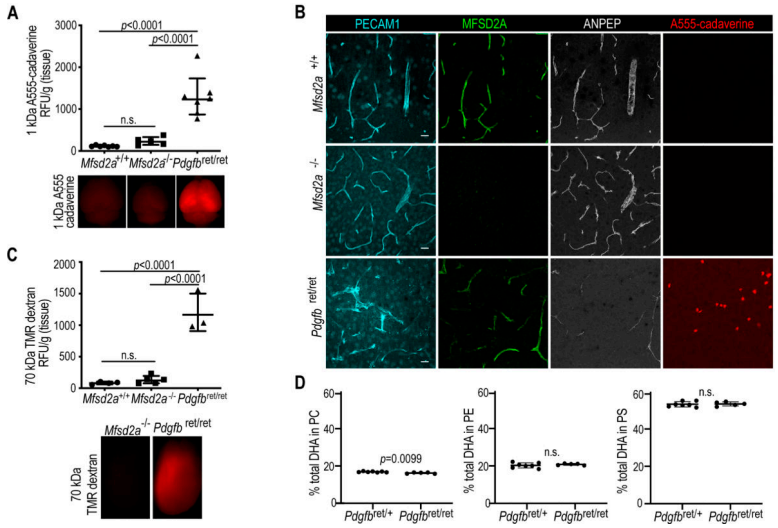

Figure 5. Lack of role of *Mfsd2a* and *Fgfbp1* in *Pdgfb*$^{ret/ret}$ BBB leakage.

A,B, Intravenously administered 1 kDa Alexa Fluor (A555) cadaverine permeability after two hours circulation in adult *Mfsd2a*$^{+/+}$, *Mfsd2a*$^{-/-}$ and *Pdgfb*$^{ret/ret}$ mice. **A,** Graph shows quantification of extravasated tracer in the brain (*Mfsd2a*$^{+/+}$ n=7, *Mfsd2a*$^{-/-}$ n=5 and *Pdgfb*$^{ret/ret}$ n=7). Lower panel shows whole brains photographed after tracer circulation. **B,** Three-dimensional reconstructions of confocal image z-stacks of cerebral neocortex vasculature IF stained as indicated. Extravasated A555-cadaverine accumulates in neurons.[17] Scale bar 20 μm. **C,** 70 kDa TMR-dextran accumulation into brains after 16-hour circulation. Lower panel illustrates whole brains photographed after tracer circulation. (*Mfsd2a*$^{+/+}$ n=4, *Mfsd2a*$^{-/-}$ n=5 and *Pdgfb*$^{ret/ret}$ n=3). **D,** Lipidomic analysis of aged *Pdgfb*$^{ret/ret}$ and *Pdgfb*$^{ret/ret}$ brains (*Pdgfb*$^{ret/+}$ n=7, *Pdgfb*$^{ret/ret}$ n=6). DHA- docosahexaenoic acid, PC-phosphatidylcholin, PE- phosphatidylethanolamine, PS- phosphatidylserine. Data in **A,C** were normally distributed and significance was evaluated using One-way ANOVA with Bonferroni's multiple comparison test. Significance in **D** was evaluated using unpaired two-tailed t-test with Welch's correction. Data are presented as geometric mean ± geometric SD. n.s.=not significant.

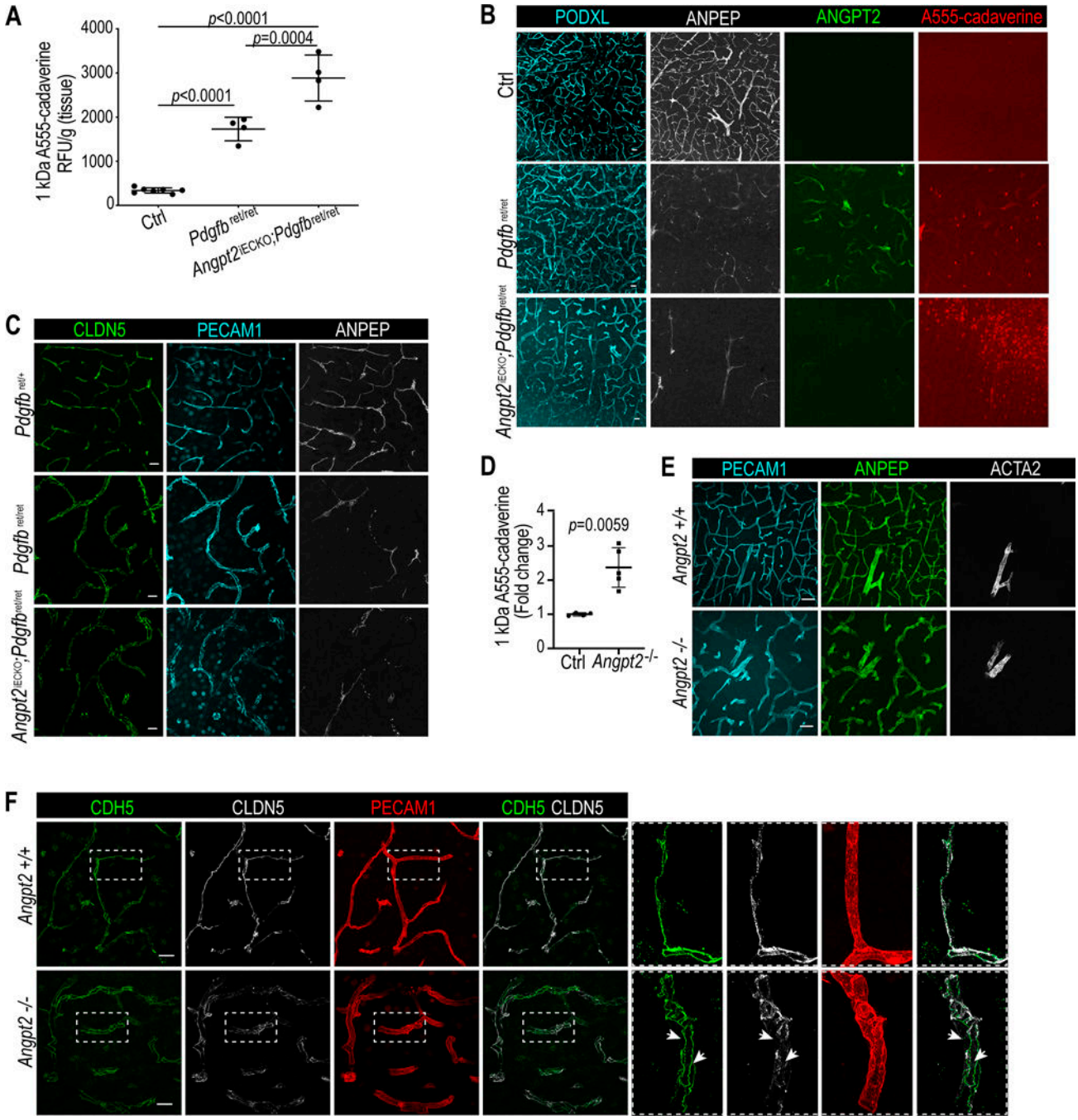

Figure 6. Role of *Angpt2* at the BBB.

A, Quantification of A555-cadaverine extravasation into brain tissue (Ctrl n=8, *Pdgfb*$^{ret/ret}$ n=4, *Angpt2*^{iECKO}*;Pdgfb*$^{ret/ret}$ n=4, control genotypes provided in Methods). **B,** Three-dimensional reconstruction of confocal image z-stacks of cerebral neocortex vasculature depicted by IF staining as indicated in *Ctrl*, *Pdgfb*$^{ret/ret}$ and *Angpt2*^{iECKO}*;Pdgfb*$^{ret/ret}$ mice. Extravasated A555-cadaverine accumulates in neurons. Scale bar 20 μm. **C,** CLDN5 distribution is irregular in both *Pdgfb*$^{ret/ret}$ and *Angpt2*^{iECKO}*;Pdgfb*$^{ret/ret}$ brains. Scale bar 20 μm. **D,** Quantification of the A555- cadaverine extravasation into brain tissue (Ctrl n=4,

Angpt2$^{-/-}$ n=5, control genotypes are provided in Methods). **E,** Representative images of the vascular mural cell coverage in cerebral cortex (n=3). Scale bar 40 μm. **F,** Representative images of the CDH5 and CLDN5 junctional distribution in EC in cerebral cortex (n=3). Insets in *Angpt2*$^{+/+}$ illustrate continuous and overlapping CDH5 and CLDN5, whereas insets in *Angpt2*$^{-/-}$ panel show continuous CDH5 but discontinuous CLDN5 (arrows). Scale bar 20 μm. Data in **A** and **D** was normally distributed and significance evaluated using One-way ANOVA with Bonferroni's multiple comparison test. Data are presented as geometric mean ± geometric SD.